Five Special Types of Orbits Around Mars

Xiaodong Liu[1], Hexi Baoyin[2], and Xingrui Ma[3]

Department of Aerospace Engineering, Tsinghua University, Beijing 100084 CHINA

Nomenclature

a = semimajor axis, km

e = orbital eccentricity

i = orbital inclination, deg.

J_2 = second order zonal harmonic

J_3 = third order zonal harmonic

J_4 = fourth order zonal harmonic

J_{22} = second degree and order tesseral harmonic

M = mean anomaly, deg.

n = mean angular velocity, s^{-1}

n_s = Mars's mean motion around the sun

p = semiparameter, km

R_e = reference radius of Mars, km

r = position of the spacecraft, km

T = orbital period, days

ω = argument of perigee, deg.

ω_m = rotational angular speed of Mars

[1] PhD candidate, Department of Aerospace Engineering, Tsinghua University
[2] Associate Professor, Department of Aerospace Engineering, Tsinghua University
[3] Professor, Department of Aerospace Engineering, Tsinghua University

Ω = right ascension of the ascending node, deg.

λ = latitude of body-fixed coordinate system

λ_{22} = longitude of the major axis of the elliptical equator

μ = Martian gravitational constant, km^3/s^2

φ = longitude of body-fixed coordinate system

Superscripts

$\bar{}$ = average value

I. Introduction

Mars's similarity to Earth has aroused considerable curiosity for a long time. Recently, interest in searching for evidence that water and extraterrestrial life previously existed on Mars has made the planet a major target of planetary exploration.

Since the 1990s, several Mars-orbiting space missions have been launched, such as Mars Global Surveyor (MGS) [1] and Mars Reconnaissance Orbiter (MRO) [2]; additional Mars exploration missions are currently being planned, such as Mars Atmosphere and Volatile Evolution [3] and Mars Trace Gas Mission. For these missions, orbit design is a very important issue, and research in this area is vitally important for the success of these missions.

Typically, satellites orbiting around a celestial body are placed into one of five special types of orbits: sun-synchronous orbits, orbits at the critical inclination, frozen orbits, repeating ground track orbits, and areostationary orbits. Sun-synchronous orbits are orbits with a precession rate of the orbital plane equal to the planetary revolution around the sun, so these orbits are especially suitable for remote sensing satellites.

Lagrangian planetary equations, which give the mean precession rate of the line of node, provide the theoretical foundation of sun-synchronous orbits. Boain described basic mechanical characteristics of Earth's sun-synchronous orbits and provided several design algorithms to satisfy practical mission requirements [4]. Several Martian satellites have been placed into sun-synchronous orbits, such as MGS [1] and MRO [2].

Orbits at the critical inclination can keep eccentricity and argument of perigee invariable on average. For example, the Molniya and Tundra orbits applied such conditions to stop the rotation of argument of perigee. Orlov introduced the concept of the Earth critical inclination [5], and Brouwer eliminated short-period terms based on canonical transformations [6]. Later, Coffey analyzed the averaged Hamilton system reduced by the Delaunay normalization and provided geometrical interpretation of the critical inclination for Earth's artificial satellites [7]. Some research has regarded orbits at the critical inclination as types of frozen orbits [8, 9].

Frozen orbits have always been an important focus of orbit design because their average eccentricity and argument of perigee remain constant. Cutting first proposed the idea of frozen orbits in his research regarding orbit analysis of the Earth satellite SEASAT-A [10]. Coffey discovered three families of frozen orbits in the averaged zonal problem up to J_9 for satellites close to an Earth-like planet [8]. Aorpimai analyzed the conditions of Earth frozen orbits using epicycle elements, and he extended analytic analysis to arbitrary zonal terms [9]. Folta used numerical simulations combined with a traditional differential correction (DC) process to obtain frozen orbits around the moon in the full gravity model [11].

Repeating ground track orbits are defined as orbits with periodically repeating ground tracks, meaning that the trajectory ground track will repeat after a whole number of revolutions within a whole number of days. A repeating ground track is the key factor for the temporal resolution of Earth satellites, and this concept is one of the major design considerations of sun-synchronous orbits [4]. Earth's satellites are often placed into repeating ground track orbits in order to achieve better coverage properties [12, 13].

Stationary orbits around Mars are usually referred to as areostationary orbits, even though no satellites have been placed in these orbits so far. However, stationary orbits around Earth have been widely used, especially for communications satellites and navigation satellites. Clarke proposed the notion of stationary orbits for Earth, and he considered it applicable for communications satellites [14]. Musen and Bailie proved that there exist four equilibrium solutions for geostationary orbits: two are stable and two are unstable [15]. Elipe and López-Moratalla analyzed the stability of the stationary points for any celestial body [16].

In the present study, analytical formulations and numerical simulations are used to analyze these five types of orbits around Mars. The analytical formulations are based on mean element theory, for which Kozai [17], Brouwer [18], Lyddane [19], and Iszak [20] contributed research. For the numerical verifications, PSODE algorithm, which combines particle swarm optimization (PSO) with differential evolution (DE) [21], is used. The only perturbation considered is the gravitational asphericity effect because this is the most basic factor that encourages or influences these orbits. Other perturbations, including atmospheric forces, solar gravitational force, and solar radiation pressure, are not considered.

This study investigates characteristics of five special types of Martian orbits, and provides analytical and numerical methods to achieve them. These orbits are also compared with their Earth counterparts. It is expected that the survey results could be useful for the orbit design of future Mars exploration missions.

II. Mars Gravity Model

The Mars gravity model used in this study is Goddard Mars Model 2B (GMM-2B), which contains spherical harmonic coefficients up to 80×80 [22]. Some of the zonal harmonics and tesserals used are given as J_2=1.95545×10^{-3}, J_3=3.14498×10^{-5}, J_4=-1.53774×10^{-5}, J_{22}=6.30692×10^{-5}, $\lambda_{22}=74.7447°$. For Earth, these zonal harmonics and tesserals are given as J_2=1.08263×10^{-3}, J_3= – 2.53266×10^{-6}, J_4= – 1.61962×10^{-5}, J_{22}=1.81534×10^{-6}, $\lambda_{22}=-14.9288°$ [23].

It is clear that the term of oblateness J_2 of Mars is dominant among the harmonic coefficients, but it is not as dominant as Earth's J_2. The other first few harmonic coefficients are also strong for Mars: about 1–2 orders of magnitude lower than J_2; for Earth, the other first few harmonic coefficients are about 3–4 orders of magnitude lower than J_2. Due to these characteristics, the motion of spacecraft orbiting around Mars and Earth will be quite different.

III. Mean Element Theory

The motion of a spacecraft under gravitational perturbation can be described using mean element theory, which is a modified perturbation method. It divides the perturbation variables into three different terms: secular terms, long-period terms, and

short-period terms, and it approximates satellite motion by separating periodic terms from secular terms [17, 18]. In this study, analytical formulations contain periodic perturbations of the first order and secular perturbations up to the second order.

IV. Sun-synchronous Orbits

Mars has a richly aspherical gravity field, with swelling at the equator. The equatorial bulge is responsible for the fact that the line of node, which is the intersection of the orbital plane of the spacecraft and the Mars equatorial plane, remains in constant rotation. The changing trend can be expressed in the form of the nodal precession rate $\dot{\Omega}$.

According to mean element theory, the mean nodal precession rate is comprised of two parts: the secular perturbations of the first order and those of the second order. The nodal precession rate arising from the secular perturbations of the first order [1] is

$$\dot{\Omega}_1 = -\frac{3nJ_2R_e^2}{2a^2\left(1-e^2\right)^2}\cos i \tag{1}$$

The nodal precession rate arising from the secular perturbations of the second order [18] is

$$\begin{aligned}\dot{\Omega}_2 = -\frac{9nJ_2^2}{4p^4}\Bigg\{&\left(\frac{3}{2}+\frac{1}{6}e^2+\sqrt{1-e^2}\right)-\sin^2 i\left(\frac{5}{3}-\frac{5}{24}e^2+\frac{3}{2}\sqrt{1-e^2}\right)\\ &-\frac{35J_4}{18J_2^2}\left[\left(\frac{6}{7}+\frac{9}{7}e^2\right)-\sin^2 i\left(\frac{3}{2}+\frac{9}{4}e^2\right)\right]\Bigg\}\cos i\end{aligned} \tag{2}$$

Therefore, the mean nodal precession rate is

$$\dot{\bar{\Omega}} = \dot{\Omega}_1 + \dot{\Omega}_2 \tag{3}$$

For sun-synchronous orbits, the rate of node precession is equal to the Mars mean motion around the sun, i.e.

$$\dot{\bar{\Omega}} = n_s \tag{4}$$

This is a useful equation for achieving a wide range of sun-synchronous orbits. It can be seen that if values of a and e are set, the value of i can be determined.

Equation (4) can be further rearranged as

$$f_1(\cos i) = A_1 \cos^3 i + B_1 \cos i + C_1 = 0 \tag{5}$$

where

$$\begin{aligned} A_1 &= \frac{9nJ_2^2R_e^4}{4p^4}\left[\left(\frac{5}{3}-\frac{5}{24}e^2+\frac{3}{2}\sqrt{1-e^2}\right)-\frac{35J_4}{6J_2^2}\left(\frac{1}{2}+\frac{3}{4}e^2\right)\right] \\ B_1 &= \frac{3nJ_2R_e^2}{2p^2}\left\{1+\frac{3J_2R_e^2}{2p^2}\left[\left(-\frac{1}{6}+\frac{3}{8}e^2-\frac{1}{2}\sqrt{1-e^2}\right)+\frac{5J_4}{2J_2^2}\left(\frac{1}{2}+\frac{3}{4}e^2\right)\right]\right\} \\ C_1 &= n_s \end{aligned} \tag{6}$$

It can be seen that $f_1(\cos i)$ is the cubic function of $\cos i$, so Eq. (5) probably has one, two, or three distinct real roots in the interval $[-\pi, \pi]$. It is necessary to judge whether all roots of Eq. (5) are meaningful for different semimajor axes. Based on the theory of the cubic equation, Eq. (5) has three real roots only if the discriminant satisfies the condition

$$\Delta = \frac{C_1^2}{4A_1^2} + \frac{B_1^3}{27A_1^3} \le 0 \tag{7}$$

Additionally, in order to avoid impact with the Martian surface, eccentricity should yield

$$e < 1 - R_e / a \tag{8}$$

Figure 1 shows the values of the discriminant for $a \in [3497, 103397]\,km$ and $e \in [0, 1-R_e/a]$. Note that the values of the discriminant are always greater than zero. Therefore, it is concluded that Eq. (5) has one meaningful root at the range of $a \in [3497, 103397]\,km$ and $e \in [0, 1-R_e/a]$; in other words, the conditions for three

roots will result in an impact with the surface of Mars. Thus, it is evident that there usually exists only one sun-synchronous orbit at a certain semimajor axis with normal eccentricity. Figure 2 shows a wide range of sun-synchronous circular orbits with combinations of altitudes and inclinations based on Eq. (4). It is evident that, given the same altitude, the required inclination of Martian sun-synchronous orbits is always smaller than Earth's.

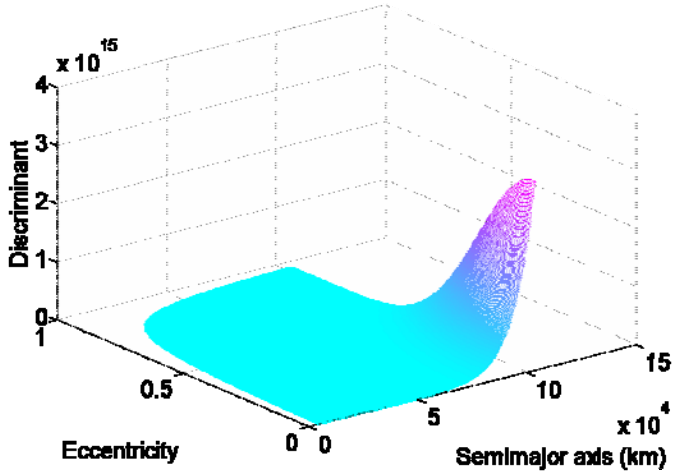

Fig. 1 The discriminant of Eq. (5) for different values of semimajor axis and eccentricity

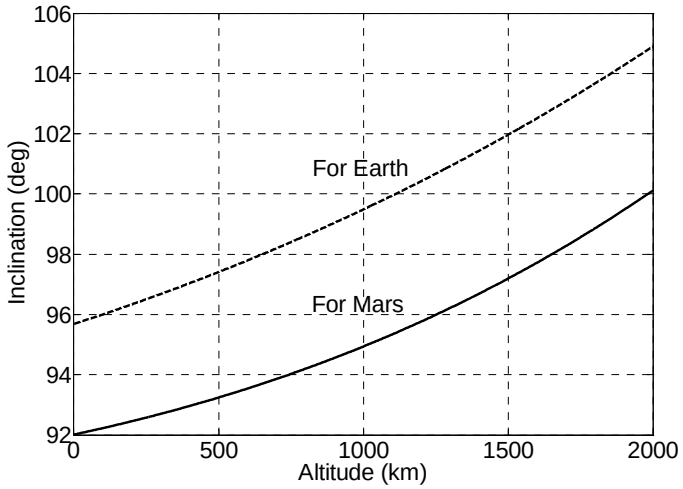

Fig. 2 Sun-synchronous altitude vs. inclination, circular orbits

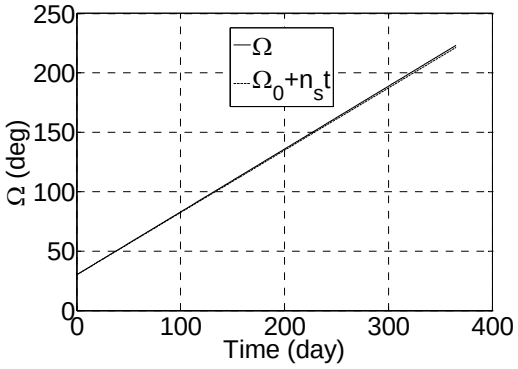

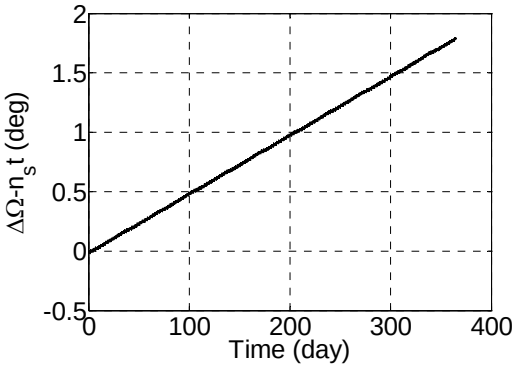

a) Evolution of Ω for $i = 93.242°$ b) Difference between $\Delta\Omega$ and $n_s t$ for $i = 93.242°$

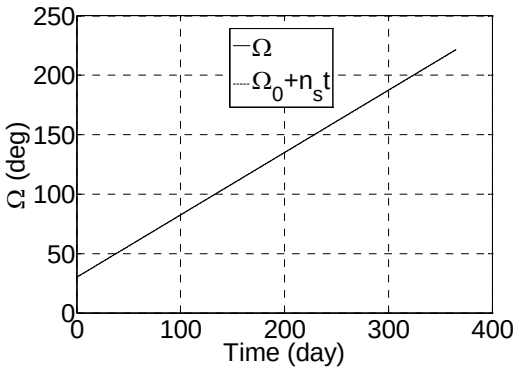

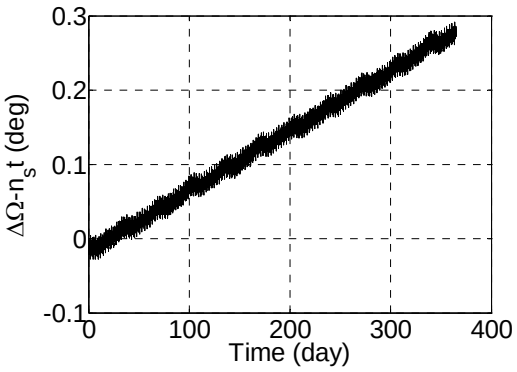

c) Evolution of Ω for $i = 93.216°$ d) Difference between $\Delta\Omega$ and $n_s t$ for $i = 93.216°$

Fig. 3 Evolution of Ω and the difference between $\Delta\Omega$ and $n_s t$ over one year for $a = 3897\ km$ and $i = 93.242°,\ 93.216°$.

For Martian sun-synchronous circular orbits, when $a = 3897\ km$, the corresponding i is $93.242°$ based on Eq. (4). Figure 3a shows the evolution of Ω for a sun-synchronous orbit with this inclination, and Fig. 3b shows that the difference between the variations of the right ascension of the ascending node and Mars's rotation angle around the sun is about $1.8°$ over one year.

By applying PSODE algorithm with inclination as the optimized variable, the difference between the variations of the right ascension of the ascending node and Mars's rotation angle around the sun are reduced further. The optimized i is obtained as $93.216°$ when $a = 3897\,km$. Figure 3c shows the evolution of Ω over one year with this inclination, and Fig. 3d shows that the difference between the variations of the right ascension of the ascending node and Mars's rotation angle around the sun is about $0.29°$ over one year. Comparing Fig. 3b and Fig. 3d, it is evident that the optimization under the full gravity field significantly improves the synchronous characteristics. The difference in i between the analytical and numerical solutions is $0.026°$, corresponding to the position precision of the spacecraft at about $1.8\,km$. This position precision can be achieved at present.

V. Orbits at the Critical Inclination

The Martian equatorial bulge can lead to rotation of argument of perigee and variation of eccentricity, which will negatively affect missions to Mars. These disadvantages can be avoided by selecting orbits at the critical inclination.

The traditional method for analyzing orbits at the critical inclination only considers the J_2 term, i.e. the secular perturbations of the first order. Using this method, the average variation rates of eccentricity and argument of perigee are

$$\dot{e}_1 = 0 \tag{9}$$

$$\dot{\omega}_1 = -\frac{3nJ_2R_2^2}{2a^2(1-e^2)^2}\left(\frac{5}{2}\sin^2 i - 2\right) \tag{10}$$

The condition that the drift rate of the mean eccentricity equals zero is naturally met, and rotation of argument of perigee can be stopped if the inclination satisfies the equation

$$\frac{5}{2}\sin^2 i - 2 = 0 \tag{11}$$

Thus, the critical inclination in the traditional sense is

$$i \cong 63.435^\circ \left(\text{or } 116.565^\circ\right) \tag{12}$$

The method mentioned above is useful for Earth, but it is not accurate enough for Mars because of special properties of the Mars gravity field, where the J_2 term does not exceed J_3 by even one hundred times. By contrast, in Earth's gravity field, J_2 exceeds J_3 by more than one thousand times. The changes of e and ω over one year are shown by the phase space diagram (where e is radial and ω is counter-clockwise) in Fig. 4 for $i = 63.435^\circ$. It can be seen that ω keeps rotating during the year, the magnitude of which is approximately 30°.

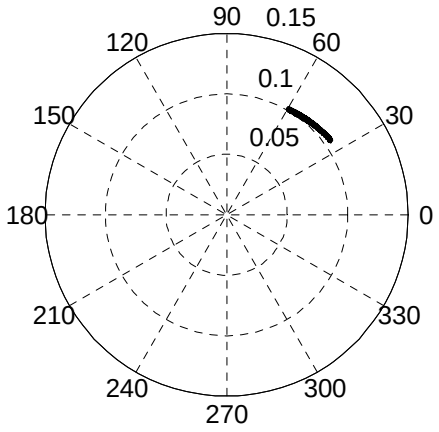

Fig. 4 $e-\omega$ evolution over one year for $i = 63.435^\circ$

In order to find a better initial condition, the secular perturbations of the second order need to be considered in addition to those of the first order. The average variation rates of e and ω arising from the secular perturbations of the second order are [18]

$$\dot{e}_2 = 0 \tag{13}$$

$$\begin{aligned}\dot{\omega}_2 = \frac{9nJ_2^2R_e^4}{p^4}\Bigg\{&\left(4+\frac{7}{12}e^2+2\sqrt{1-e^2}\right)-\sin^2 i\left(\frac{103}{12}+\frac{3}{8}e^2+\frac{11}{2}\sqrt{1-e^2}\right)+\\ &\sin^4 i\left(\frac{215}{48}-\frac{15}{32}e^2+\frac{15}{4}\sqrt{1-e^2}\right)-\\ &\frac{35J_4}{18J_2^2}\left[\left(\frac{12}{7}+\frac{27}{14}e^2\right)-\sin^2 i\left(\frac{93}{14}+\frac{27}{4}e^2\right)+\sin^4 i\left(\frac{21}{4}+\frac{81}{16}e^2\right)\right]\Bigg\}\end{aligned} \tag{14}$$

The condition of Eq. (13) is also naturally met, so only the average variation rate of ω needs to be considered, and is set equal to zero.

$$\dot{\bar{\omega}} = \dot{\omega}_1 + \dot{\omega}_2 = 0 \tag{15}$$

Substituting Eqs. (10) and (14) into (15), Eq. (15) can be rearranged as

$$f_2\left(\sin^2 i\right) = A_2 \sin^4 i + B_2 \sin^2 i + C_2 = 0 \tag{16}$$

where

$$\begin{aligned}A_2 &= \frac{9nJ_2^2R_e^4}{4p^4}\left[\left(\frac{215}{48}-\frac{15}{32}e^2+\frac{15}{4}\sqrt{1-e^2}\right)-\frac{35J_4}{18J_2^2}\left(\frac{21}{4}+\frac{81}{16}e^2\right)\right]\\ B_2 &= \frac{3nJ_2R_e^2}{4p^2}\left\{-5+\frac{3J_2R_e^2}{p^2}\left[-\left(\frac{103}{12}+\frac{3}{8}e^2+\frac{11}{2}\sqrt{1-e^2}\right)+\frac{35J_4}{6J_2^2}\left(\frac{31}{14}+\frac{9}{4}e^2\right)\right]\right\}\\ C_2 &= \frac{3nJ_2R_e^2}{4p^2}\left\{4+\frac{3J_2R_e^2}{p^2}\left[\left(4+\frac{7}{12}e^2+2\sqrt{1-e^2}\right)-\frac{5J_4}{6J_2^2}\left(4+\frac{9}{2}e^2\right)\right]\right\}\end{aligned} \tag{17}$$

It can be seen that $f_2\left(\sin^2 i\right)$ is the quadratic function of $\sin^2 i$, so Eq. (16) may have two or four real roots in the interval $[-\pi, \pi]$. It is necessary to clarify whether all roots of Eq. (16) are meaningful for different semimajor axes. Setting $x = \sin^2 i$, Eq. (16) can be rewritten as

$$f_2(x) = A_2 x^2 + B_2 x + C_2 = 0 \tag{18}$$

So the condition that Eq. (16) has four real roots in the interval $[-\pi, \pi]$ is equivalent to the condition that Eq. (18) has two distinct real roots in the interval $[0,1]$. It can be easily proved that $A_2 > 0$, $B_2 < 0$, and $C_2 > 0$ for Mars. Thus, Eq. (18) has two distinct real roots in the in the interval $[0,1]$ only if

$$f_2(1) = A_2 + B_2 + C_2 > 0 \tag{19}$$

Additionally, in order to avoid an impact on the Martian surface, eccentricity should satisfy the inequality (8). Figure 5 shows the values of $f_2(1)$ for $a \in [3497, 103397]\, km$ and $e \in [0, 1 - R_e / a]$. Note that the values of $f_2(1)$ in Fig. 5 are always less than zero, which means that Eq. (18) has only one root in the interval $[0,1]$. It can be concluded that there exist two critical inclinations at the given wide range of a and e, and that the conditions for the four critical inclinations will result in a Martian impact.

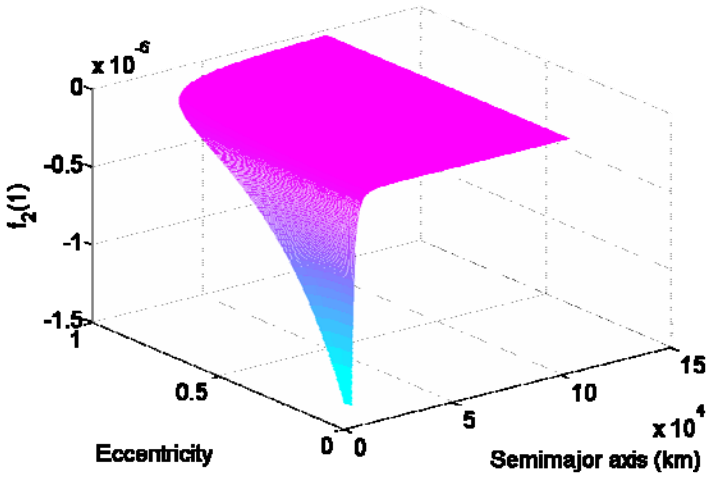

Fig. 5 $f_2(1)$ as a function of the semimajor axis and eccentricity

For Earth, the same critical inclinations 63.435° and 116.565° exist for different semimajor axes and eccentricities, while for Mars, the critical inclinations are a function

of the semimajor axes and eccentricities. For example, if $a = 3897km$ and $e = 0.1$, the critical inclinations are $63.310°$ and $116.690°$. Figure 6a presents $e - \omega$ evolution over one year for $i = 63.310°$, and it shows that excursions in e and ω are reduced.

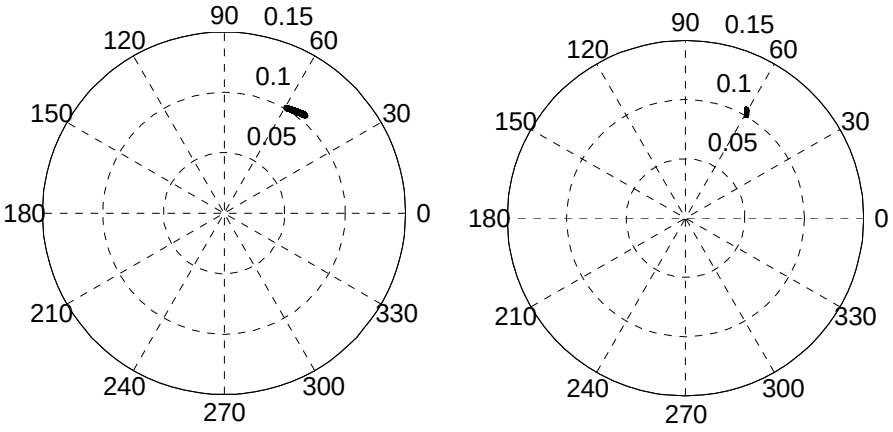

a) $e - \omega$ evolution for $i = 63.310°$. b) $e - \omega$ evolution for $i = 63.311°$

Fig. 6 $e - \omega$ evolution over one year.

By employing PSODE algorithm with i as the optimized variable in the full gravity field, an optimized critical inclination is found, i.e. $i = 63.311°$. Figure 6b presents $e - \omega$ evolution over one year for the optimized critical inclination. It can be seen that excursions in e and ω maintain their local location over one year without any maintenance. The difference in inclination between analytical and optimized solutions is only $0.001°$, corresponding to the position precision of the spacecraft at approximately $70\,m$. To gain the benefit shown, it would be required to navigate to this level of precision, the feasibility of which depends on the navigation performance of the spacecraft.

VI. Frozen Orbits

To keep e and ω constant on average, frozen orbits are also advantageous because a and i can be set independently. For frozen orbits, the variations of e and ω can be stopped by choosing a small eccentricity and argument of perigee to be around either $90°$ or $270°$.

Because of the small eccentricity, long-period terms of the first order must be considered. The main parts of the first order long-period terms of e and ω [18] are

$$e_l^{(1)} = -\frac{J_3 R_e}{2J_2 p}\sin i\left(1-e^2\right)\sin\omega \tag{20}$$

$$\omega_l^{(1)} = -\frac{J_3 R_e}{2J_2 p}\left(\frac{\sin i - e^2\cos^2 i}{\sin i}\right)\frac{\cos\omega}{e} \tag{21}$$

Thus, the average variation rates of e and ω are given by

$$\dot{\bar{e}} = \dot{e}_1 + \dot{e}_l^{(1)} + \dot{e}_2 = \dot{e}_l^{(1)} = \frac{3nJ_3R_e^3\sin i}{4a^3\left(1-e^2\right)^2}\left(\frac{5}{2}\sin^2 i - 2\right)\cos\omega \tag{22}$$

$$\begin{aligned}\dot{\bar{\omega}} &= \dot{\omega}_1 + \dot{\omega}_l^{(1)} + \dot{\omega}_2 \\ &= \frac{3nJ_2R_e^2}{2p^2}\left\{\left(2-\frac{5}{2}\sin^2 i\right)\left[1+\frac{J_3R_e}{2J_2p}\left(\frac{\sin^2 i - e^2\cos^2 i}{\sin i}\right)\frac{\sin\omega}{e}\right]+\frac{3J_2R_e^2}{2p^2}D\right\}\end{aligned} \tag{23}$$

where

$$\begin{aligned}D = &\left(4+\frac{7}{12}e^2+2\sqrt{1-e^2}\right)-\sin^2 i\left(\frac{103}{12}+\frac{3}{8}e^2+\frac{11}{2}\sqrt{1-e^2}\right)+\sin^4 i\left(\frac{215}{48}-\frac{15}{32}e^2+\frac{15}{4}\sqrt{1-e^2}\right) \\ &-\frac{35J_4}{18J_2^2}\left[\left(\frac{12}{7}+\frac{27}{14}e^2\right)-\sin^2 i\left(\frac{93}{14}+\frac{27}{4}e^2\right)+\sin^4 i\left(\frac{21}{4}+\frac{81}{16}e^2\right)\right]\end{aligned} \tag{24}$$

For frozen orbits, the average variation rates of e and ω are set equal to zero.

$$\dot{\bar{e}} = 0 \tag{25}$$

$$\dot{\bar{\omega}} = 0 \tag{26}$$

Solving Eqs. (25) and (26) where it is approximated that $e^2 \approx 0$, the required e and ω are obtained as

$$e = -\frac{\dfrac{J_3 R_e}{2J_2 a}\sin i \sin\omega}{1-\dfrac{3J_2 R_e^2 E}{a^2\left(5\sin^2 i - 4\right)}} \tag{27}$$

$$\omega = 90^\circ \text{ or } 270^\circ \tag{28}$$

where

$$E = \left(6 - \frac{169}{12}\sin^2 i + \frac{395}{48}\sin^4 i\right) - \frac{35J_4}{18J_2^2}\left(\frac{12}{7} - \frac{93}{14}\sin^2 i + \frac{21}{4}\sin^4 i\right) \tag{29}$$

From the above analysis, it can be seen that a and i can be set independently for frozen orbits, which will provide great convenience for different missions. Figure 7 shows values of frozen e for combinations of a and i. Here, the twin peaks correspond to zeros of the denominator of Eq. (27).

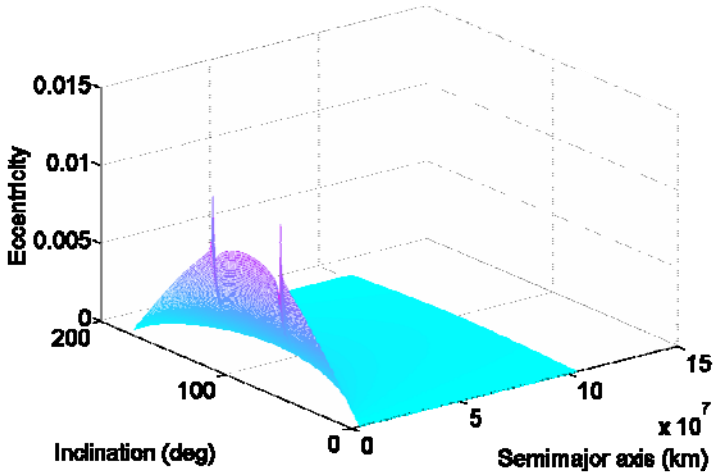

Fig. 7 Frozen eccentricity as a function of the semimajor axis and inclination.

In order to make e meaningful, ω must be set to about 90° for Earth because J_2 and J_3 have the opposite sign; otherwise, e is negative. For Mars, ω must be set to around 270° because J_2 and J_3 have the same sign. If given $a = 3897\ km$ and $i = 60°$, the corresponding e is 0.0063414 and ω is 270° based on Eqs. (27) and (28). This result achieves a good property as an approximate frozen orbit in the full gravity field, as shown in Fig. 8a.

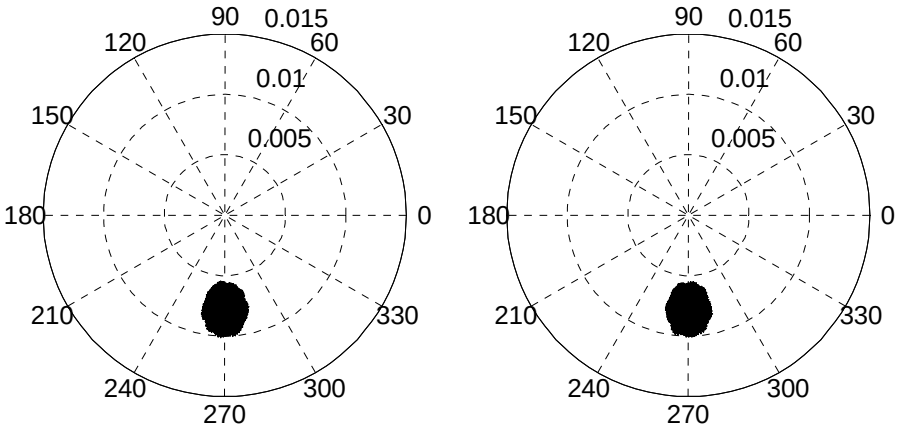

a) $\omega = 270°$, $e = 0.0063414$ b) $\omega = 270.54477°$, $e = 0.0075389$

Fig. 8 $e - \omega$ evolution over one year for different e and ω.

Using PSODE algorithm with e and ω as optimized variables, the optimized e and ω are obtained, where $e = 0.0075389$ and $\omega = 270.54477°$. Figure 8b presents the evolutions of e and ω. It can be seen that the numerical solution is close to the analytical solution, and the variations of e and ω are not minimized significantly after applying PSODE algorithm. Therefore, analytical formulations can provide good initial conditions for Martian frozen orbits.

VII. Repeating Ground Track Orbits

Repeating ground track orbits have the valuable property that their ground track repeats periodically. These orbits can provide good appearance for orbital covering, which is significant for remote sensing satellites.

For a satellite, the interval of the adjacent ground track in the equator is

$$\Delta\lambda = T_N\left(\omega_M - \dot{\bar{\Omega}}\right) \tag{30}$$

where T_N is the nodal period of the motion of the spacecraft, which can be expressed as

$$T_N = \frac{2\pi}{\dot{\bar{M}} + \dot{\bar{\omega}}} \tag{31}$$

Based on mean element theory, the average rates of Ω, M, and ω can be expressed as

$$\dot{\bar{M}} = n + \dot{M}_1 + \dot{M}_2 \tag{32}$$

$$\dot{\bar{\omega}} = \dot{\omega}_1 + \dot{\omega}_2 \tag{33}$$

$$\dot{\bar{\Omega}} = \dot{\Omega}_1 + \dot{\Omega}_2 \tag{34}$$

where [20]

$$\dot{M}_1 = \frac{3nJ_2R_e^2}{2p^2}\left(1-\frac{3}{2}\sin^2 i\right)\sqrt{1-e^2} \tag{35}$$

$$\begin{aligned}\dot{M}_2 = \frac{9nJ_2^2R_e^4}{4p^4}\sqrt{1-e^2}\Bigg\{&\frac{1}{2}\left(1-\frac{3}{2}\sin^2 i\right)^2\sqrt{1-e^2} + \left(\frac{5}{2}+\frac{10}{3}e^2\right) - \sin^2 i\left(\frac{19}{3}+\frac{26}{3}e^2\right)\\ &+\sin^4 i\left(\frac{233}{48}+\frac{103}{12}e^2\right)+\frac{e^4}{1-e^2}\left(\frac{35}{12}-\frac{35}{4}\sin^2 i+\frac{315}{32}\sin^4 i\right)\\ &-\frac{35J_4}{18J_2^2}e^2\left(\frac{9}{14}-\frac{45}{14}\sin^2 i+\frac{45}{16}\sin^4 i\right)\Bigg\}\end{aligned} \tag{36}$$

In order to realize global coverage, engineers usually adopt repeating ground track orbits whose periods are multi-sol. The condition for repeating ground track orbits can be

written as

$$RT_N\left(\omega_M - \dot{\bar{\Omega}}\right) = R \bullet \Delta\lambda = N \bullet 2\pi \tag{37}$$

or

$$RT_N = ND_N \tag{38}$$

where N and R are positive integers, and $D_N = 2\pi / \left(\omega_M - \dot{\bar{\Omega}}\right)$. In this condition, the ground track will repeat after the satellite runs R circles in N sols.

In engineering practice, the ground track repetition parameter Q is often used to describe repeating ground track orbits, which is defined as

$$Q = \frac{R}{N} \tag{39}$$

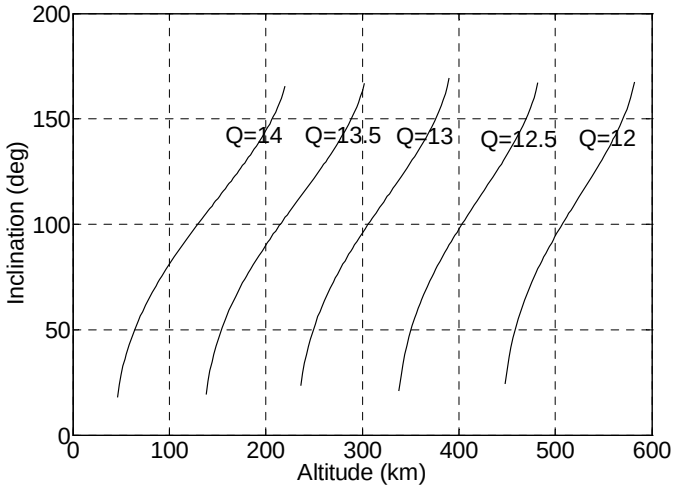

Fig. 9 Altitude vs. inclination for repeating ground track circular orbits with different Q.

Figure 9 shows the relation between altitude and inclination for repeating ground track circular orbits with different Q values. For practical planetary exploration, repeating ground track orbits are often sun-synchronous, in which case Eq. (4) must be satisfied.

Thus, if the values of R and N are fixed, a and i can be determined. For example, for a circular 5-sol repeating ground track orbit with 41 revolutions in one period, the corresponding H and i can be calculated: $H = 1627.395\,km, i = 97.809°$. It is found that the ground track was offset by $3.328°$ after five sols in the full gravity field.

By using PSODE algorithm with H and i as optimized variables, the optimized H and i can be obtained: $H = 1634.019\,km$ and $i = 97.845°$, and the offset of the ground track is reduced to $0.227°$ after five sols. Between analytical and numerical solutions, the difference in inclination is $0.036°$, corresponding to the position precision of the spacecraft at about $2.5\,km$. This position precision can be achieved at present.

VIII. Areostationary Orbits

The ground track of stationary orbits remains stationary, which arouses great interest to operators of communications and weather satellites. Extensive research has been conducted on geostationary orbits. However, the Mars gravity field is different from Earth's, which will produce distinctions in their stationary orbits.

For stationary orbits, tesseral harmonic terms (except for zonal harmonics) must be taken into account. Taking the second order and degree harmonics, the gravity potential function of Mars can be simplified as

$$U = \frac{\mu}{r}\left[1 - \frac{J_2 R_e^2}{2r^2}\left(3\sin^2\varphi - 1\right) + \frac{3J_{22}R_e^2}{r^2}\cos^2\varphi\cos 2\left(\lambda - \lambda_{22}\right)\right] \tag{40}$$

Denoting $\lambda - \lambda_{22}$ by γ, the radial, tangential, and normal motion equations of the spacecraft are, respectively,

$$\begin{cases} \ddot{r} - r\cos^2\varphi\dot{\lambda}^2 - r\dot{\varphi}^2 = -\dfrac{1}{r^2} + \dfrac{3\mu J_2 R_e^2}{2r^4}\left(3\sin^2\varphi - 1\right) - \dfrac{9\mu J_{22} R_e^2}{r^4}\cos^2\varphi\cos 2\gamma \\ \dfrac{d}{dt}\left(r^2\cos^2\varphi\dot{\lambda}\right) = -\dfrac{6\mu J_{22} R_e^2}{r^4}\cos^2\varphi\sin 2\gamma \\ \dfrac{d}{dt}\left(r^2\dot{\varphi}\right) + \dfrac{1}{2}r^2\sin 2\varphi\dot{\lambda}^2 = -\dfrac{3\mu J_2 R_e^2}{r^4}\sin\varphi\cos\varphi - \dfrac{6\mu J_{22} R_e^2}{r^4}\cos\varphi\sin\varphi\cos 2\gamma \end{cases} \tag{41}$$

From Eq. (41), it can be seen that the zonal term produces normal and radial perturbations. Normal perturbations are zero when the orbital plane is in accordance with the equatorial plane; radial perturbations increase the gravity of Mars, and thus enlarge the radius of stationary orbits. The tesseral term mainly produces tangential and radial perturbations. Tangential perturbations can lead to longitudinal drift; radial perturbations caused by the tesseral term are much smaller than those caused by the zonal term, which can always be neglected.

Four special solutions of Eq. (41) can be obtained as

$$r \equiv r_{01},\ \gamma \equiv \gamma_{01} = 90°, 270°,\ \varphi \equiv 0 \tag{42}$$

$$r \equiv r_{02},\ \gamma \equiv \gamma_{02} = 0°, 180°,\ \varphi \equiv 0 \tag{43}$$

where r_{01} and r_{02} are roots of the first expression of Eq. (41), which can be rewritten as

$$r_0\omega_m^2 = \frac{\mu}{r_0^2} + \frac{3\mu R_e^2}{r_0^4}\left(\frac{J_2}{2} \pm 3J_{22}\right) \tag{44}$$

where the signs "-" and "+" before J_{22} correspond to r_{01} and r_{02}, respectively.

The two roots r_{01} and r_{02} denote that the spacecraft is located above the minor and major axis of the elliptical equator, respectively. Substituting the Martian constants into Eq. (44), the equilibrium solutions are obtained, where $r_{01} = 20428.095533\,\text{km}$ and $r_{02} = 20428.309266\,\text{km}$.

The longitude of r_{01} is $-15.255°$ or $164.745°$, and the longitude of r_{02} is $74.745°$ or $254.745°$ (For Mars, the prime meridian is defined as the longitude of the crater 'Airy-0'.) It can be easily proved that Eqs. (42) and (43) correspond to central points and saddle points, respectively, of which the former is linear stable. For geostationary orbits, the longitude of r_{01} is $75.071°$ or $255.071°$, and the longitude of r_{02} is $-14.929°$ or $165.071°$. Let

$$\begin{aligned} r &= r_0 + \Delta r \\ \lambda &= \lambda_0 + \Delta\lambda \\ \varphi &= \varphi_0 + \Delta\varphi \\ \gamma_0 &= \lambda_0 - \lambda_{22} \end{aligned} \tag{45}$$

where λ_0, φ_0 are the initial longitude and latitude, and γ_0 is the initial angular distance from the spacecraft to the equatorial major axis. Substituting Eq. (45) into (41), the disturbance equations are derived after linearization.

$$\begin{aligned} &\Delta\ddot{r} - \left(\omega_m^2 + \frac{2\mu}{r_0^3} + \frac{6\mu J_2 R_e^2}{r_0^5} + \frac{36\mu J_{22} R_e^2}{r_0^5}\right)\Delta r - 2r_0\omega_m\Delta\dot{\lambda} - \frac{18\mu J_{22}R_e^2}{r_0^4}\Delta\lambda\sin 2\gamma_0 \\ &\quad = -\frac{\mu}{r_0^2} + r_0\omega_m^2 - \frac{3\mu J_2 R_e^2}{2r_0^4} - \frac{9\mu J_{22}R_e^2}{r_0^4}\cos 2\gamma_0 \\ &r_0\Delta\ddot{\lambda} + \frac{12\mu J_{22}R_e^2}{r_0^4}\Delta\lambda\cos 2\bar{\lambda}_0 + 2\omega_m\Delta\dot{r} - \frac{24\mu J_{22}R_e^2}{r_0^5}\Delta r\sin 2\gamma_0 \\ &\quad = -\frac{6\mu J_{22}R_e^2}{r_0^4}\sin 2\gamma_0 \\ &r_0\Delta\ddot{\varphi} + r_0\omega_m^2\Delta\varphi + \frac{3\mu J_2 R_e^2}{r_0^4}\Delta\varphi + \frac{6\mu J_{22}R_e^2}{r_0^4}\Delta\varphi\cos 2\gamma_0 = 0 \end{aligned} \tag{46}$$

It is evident from Eq. (46) that the motion in the orbital plane and the motion of the orbital plane are decoupled. Introducing new variables: $\tau = \omega_m t$, $\beta^2 = J_{22}\left(R_e / r_0\right)^2$ and $\Delta r_1 = \Delta r / r_0$, the first two expressions of Eq. (46) can be simplified as

$$\begin{aligned}&\Delta r_1'' - 3\Delta r_1 - 2\Delta\lambda' - 18\beta^2\Delta\lambda\sin 2\gamma_0 = -9\beta^2\cos 2\gamma_0\\&\Delta\lambda'' + 12\beta^2\Delta\lambda\cos 2\lambda_0 + 2\Delta r_1' - 24\beta^2\Delta r_1\sin 2\gamma_0 = -6\beta^2\sin 2\gamma_0\end{aligned} \tag{47}$$

where "'"represents the derivative with respect to τ.

The characteristic equation of Eq. (47) can be written as

$$\left(s^2 + 12\beta^2\sin 2\gamma_0 s + 1\right)\left(s^2 - 12\beta^2\sin 2\gamma_0 s - 36\beta^2\cos 2\gamma_0\right) = 0 \tag{48}$$

By approximating that $\beta^4 \approx 0$, the characteristic roots of Eq. (48) can be calculated as

$$\begin{cases} s_{1,2} = -6\beta^2\sin 2\gamma_0 \pm i \\ s_{3,4} = 6\beta^2\sin 2\gamma_0 \pm 6\beta\sqrt{\cos 2\gamma_0} \end{cases} \tag{49}$$

When the spacecraft is located above the major axis of the equator, $\cos 2\gamma_0 = 1$, where the characteristic equation contains a positive real root, so two balance positions above the major axis of the equator are unstable. When the spacecraft is located above the minor axis of the equator, $\cos 2\gamma_0 = -1$, where the roots of the characteristic equation are all pure imaginary numbers, so two balance positions above the minor axis of the equator are linear stable. From the above analysis, the deviation of the spacecraft from the minor axis is periodic. Based on the theory of ordinary differential equations, the characteristic roots $s_{1,2}$ determine the short period, which is one day; the characteristic roots $s_{3,4}$ determine the long period, which is 126.204 days. For geostationary orbits, the short period is also one day, but the long period is 819.230 days, which is much longer than that of areostationary orbits.

Taking the initial condition $r = r_{01}$, $\gamma_{01} = 90°$, and $\varphi = 0$, i.e. the point above the minor axis of the equator (longitude: $-15.255°$), the longitudinal evolution over two years can be seen in Fig. 10a. Figure 10b shows that the point located above the

equatorial minor axis is not the exact equilibrium solution in the full gravity field, and the drift amplitude is approximately $35°$.

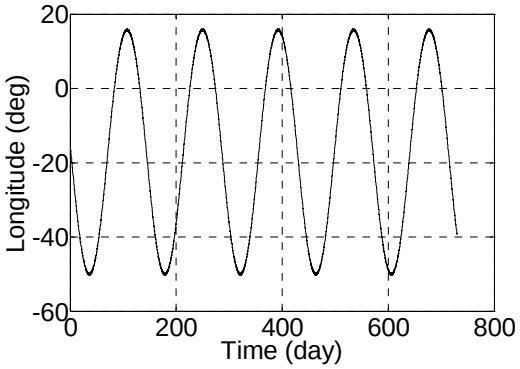

a) The point with the longitude $-15.255°$

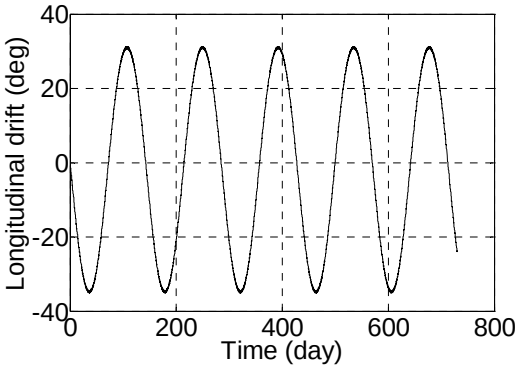

b) The point with the longitude $-15.255°$

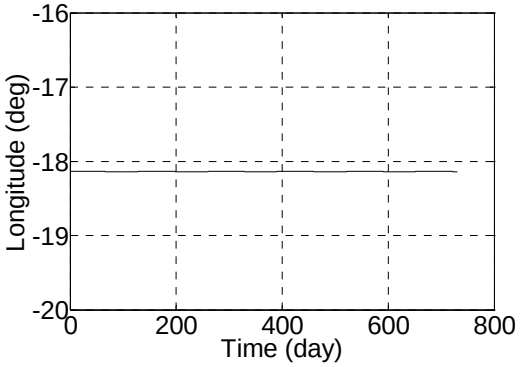

c) The point with the longitude $-18.138°$

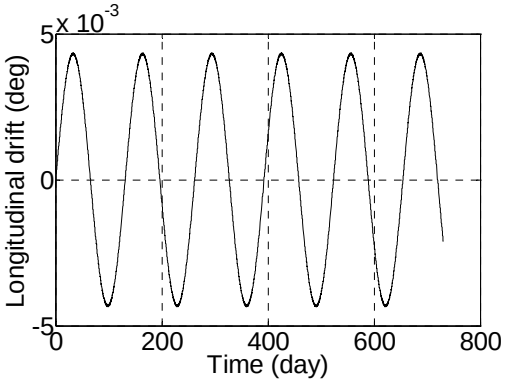

d) The point with the longitude $-18.138°$

Fig. 10 Longitudinal evolution and drift over two years for the point located above the equatorial minor axis ($\lambda = -15.255°$) and the optimized longitude ($\lambda = -18.138°$).

Using PSODE algorithm with the initial longitude of the spacecraft as the optimized variable, the more accurate equilibrium solution can be obtained, which is near to the point located above the equatorial minor axis with the longitude $-18.138°$. Figure 10c presents two years' simulation, and it shows that this point is the exact equilibrium solution in the full gravity field. Figure 10d shows that after optimization, the amplitude

of the longitude can be reduced significantly, to about $0.00435°$. Thus, the point with the longitude $-18.138°$ can be used as the initial condition for areostationary orbits, where stationkeeping is not necessary.

IX. Conclusions

There exist five special types of orbits around Mars: sun-synchronous orbits, orbits at the critical inclination, frozen orbits, repeating ground track orbits, and areostationary orbits. The constraint conditions for achieving these special orbits have been found based on analytical formulations and numerical simulations in an 80×80 Mars gravity field. It has been shown that the behaviors of these orbits are different from those of their Earth counterparts. Martian sun-synchronous orbits may have one, two, or three distinct inclinations when given semimajor axis and eccentricity. However, only one meaningful inclination exists; the other inclinations might be expected to result in an impact with the Martian surface. The required inclination of Martian sun-synchronous orbits is always smaller than that of Earth's with the same altitude. For Mars, critical inclinations are functions of the semimajor axis and eccentricity. For a given semimajor axis and eccentricity, there may exist either two or four critical inclinations. However, only the two critical inclinations are meaningful; the four critical inclinations might result in an impact with the Martian surface. Martian frozen orbits always have small eccentricity, and argument of perigee must be set to approximately $270°$, while for Earth, argument of perigee must be set to about $90°$. Repeating ground track orbits around about Mars can also be realized, and in engineering practice, they are often sun-synchronous. For satellites orbiting around Mars, there exist four stationary solutions, two stable and two unstable. Stable solutions are located at the minor axis of the elliptical equator, making

areostationary orbits possible. The long oscillation period of areostationary orbits is about 126 days, which is much shorter than that of geostationary orbits.

The analysis also shows that the restrictive definition of these orbits cannot be precisely satisfied in the 80×80 Mars gravity field, but it is possible to select these special orbits for Mars that can reduce or eliminate the need for stationkeeping. These orbits are of special interest for missions around Mars and are appropriate for various requirements. It is expected that this study can provide orbit design principles for future Mars exploration missions.

Acknowledgements

This research was supported by the National Natural Science Foundation of China (No. 10832004 and No. 10602027). Thanks to Alexander J. Grubb, Chief English Editor, Native Tongue Language Services, for his assistance with this article.

References

[1] Lyons, D. T., Beerer, J. G., Esposito, P., Johnston, M. D., and Willcockson, W. T., "Mars Global Surveyor: Aerobraking Mission Overview," *Journal of Spacecraft and Rockets*, Vol. 36, No. 3, 1999, pp. 307–313. doi: 10.2514/2.3472.

[2] Jai, B., Wenkert, D., Hammer, B., Carlton, M., Johnston, D., and Halbrook, T., "An Overview of Mars Reconnaissance Orbiter Mission, and Operations Challenges," AIAA SPACE 2007 Conference and Exposition, Long Beach, CA, AIAA Paper 2007-6090, Sept. 2007.

[3] Jakosky, B. M., "The 2013 Mars Atmosphere and Volatile Evolution (MAVEN) Mission to Mars," American Geophysical Union, Fall Meeting, American Geophysical Union Paper P11B-1211, 2009.

[4] Boain, R. J., "A-B-Cs of Sun-Synchronous Orbit Mission Design," *Advances in the Astronautical Sciences*, Vol. 119, Part 1, 2004, pp. 85–104.

[5] Orlov, A. A., "Pochti Krugovye Periodicheskie Dvizheniia Materialnoi Tochki Pod Deistviem Niutonovskogo Pritiazheniia Sferoida," *Soobshcheniia Gosudarstvennogo astronomicheskogo instituta imeni P.K. Shternberga*, 1953, No. 88–89, pp. 3–38.

[6] Brouwer, D., "Outlines of General Theories of the Hill-Brown and Delaunay Types for Orbits of Artificial Satellites," *The Astronomical Journal*, 1958, Vol. 63, pp. 433–438.

[7] Coffey, S. L., Deprit, A., and Miller, B. L., "The Critical Inclination in Artificial Satellite Theory," *Celestial Mechanics and Dynamical Astronomy*, Vol. 39, No. 4, Dec. 1986, pp. 365–406. doi: 10.1007/BF01230483.

[8] Coffey, S. L., Deprit, A., and Deprit, E., "Frozen Orbits for Satellites Close to an Earth-like Planet," *Celestial Mechanics and Dynamical Astronomy*, Vol. 59, No.1, 1994, pp. 37–72. doi: 10.1007/BF00691970.

[9] Aorpimai, M., and Palmer P. L., "Analysis of Frozen Conditions and Optimal Frozen Orbit Insertion," *Journal of Guidance, Control, and Dynamics*, Vol. 26, No. 5, 2003, pp. 786–793. doi: 10.2514/2.5113.

[10] Cutting, E., Born, G. H., and Frautnick, J. C., "Orbit Analysis For SEASAT-A," *Journal of the Astronautical Sciences*, Vol. 26, No. 4, 1978, pp. 315–342.

[11] Folta, D., and Quinn, D., "Lunar Frozen Orbits," AIAA/AAS Astrodynamics Specialist Conference and Exhibit, Keystone, CO, AIAA Paper 2006-6749, Aug. 2006.

[12] Zhang, J., He, X. S., Li, L., Deng, F. Y., and Zhang, Y. F., "Designing LEO Retrograde Orbit Twin-Station Satellite Constellation for Regional Coverage," 25th AIAA International Communications Satellite Systems Conference, Seoul, South Korea, AIAA Paper 2007-3305, April 2007.

[13] Pontani, M., and Teofilatto, P., “Satellite Constellations for Continuous and Early Warning Observation: A Correlation-Based Approach,” *Journal of Guidance, Control, and Dynamics*, Vol. 30, No. 4, 2007, pp. 910–920. doi: 10.2514/1.23094.

[14] Clarke, A. C., “Extra-Terrestrial Relays — Can Rocket Stations Give World-wide Radio Coverage?” *Wireless World*, Vol. 11, No. 10, Oct. 1945, pp. 305–308.

[15] Musen, P., and Bailie, A.E., “On the Motion of a 24-Hour Satellite,” *Journal of Geophysical Research*, Vol. 67, No. 3, 1962, pp. 1123–1132.

[16] Elipe, A., and López-Moratalla, T., “On the Liapunov Stability of Stationary Points Around a Central Body,” *Journal of Guidance, Control, and Dynamics*, Vol. 29, No. 6, 2006, pp. 1376–1383.

[17] Kozai, Y., “The Motion of a Close Earth Satellite,” *The Astronomical Journal*, Vol. 64, Nov. 1959, pp. 367–377. doi: 10.1086/107957.

[18] Brouwer, D., “Solution of the Problem of Artificial Satellite Theory Without Drag,” *The Astronomical Journal*, Vol. 64, Nov. 1959, pp. 378–397. doi: 10.1086/107958.

[19] Lyddane, R. H., "Small Eccentricities or Inclinations in the Brouwer Theory of the Artificial Satellite," *The Astronomical Journal*, Vol. 68, Oct. 1963, pp.555-558.

[20] Izsak, I. G., “A Note on Perturbation Theory,” *The Astronomical Journal*, Vol. 68, Oct. 1963, pp. 559–560.

[21] Niu, B., and Li, L., “A Novel PSO-DE-Based Hybrid Algorithm for Global Optimization,” *Lecture Notes in Computer Science*, Vol. 5227, Springer-Verlag, Berlin, Heidelberg, 2008, pp. 156–163. doi: 10.1007/978-3-540-85984-0.

[22] Lemoine, F.G., Smith,D. E., Rowlands,D. D., Zuber,M. T.,Neumann, G. A., Chinn, D. S., and Pavlis, D. E., “An Improved Solution of the Gravity Field of Mars (GMM-2B) from Mars Global Surveyor,” *Journal of Geophysical research*, Vol. 106, No. E10, 5 2001, pp. 23,359–23,376.

[23] Lemoine, F. G., Kenyon, S. C., Factor, J. K., Trimmer, R.G., Pavlis, N. K., Chinn, D. S., Cox, C. M., Klosko, S. M., Luthcke, S. B., Torrence, M. H.,Wang, Y. M.,Williamson, R. G., Pavlis, E. C., Rapp, R. H., and Olsonet, T. R., “The Development of the Joint NASA GSFC and NIMA Geopotential Model EGM96,” TM-1998-206861, 1998.